16 Thermal Contact Resistance

M. B. H. Mantelli* and M. M. Yovanovich†

Introduction

In vacuum environments on spacecraft, convective heat transfer is absent and conduction becomes a more important heat-transfer mechanism than it is for most terrestrial hardware. The heat generated by piece parts within a spacecraft electronics box must flow, by conduction, to the box surface, where it is either radiated away or conducted to a heat sink. Included in this conductive path are a number of joints where heat must be transferred by contact between surfaces. These joints include screws or Wedglock guides that attach circuit boards to an electronics-box chassis, and bolts used to attach the electronics box to a spacecraft shelf or heat-pipe network. Hence the thermal conductance of contacting surfaces is an important parameter for spacecraft thermal design.

This chapter presents analytical tools for modeling thermal joint resistance (or its inverse, conductance) between contacting surfaces. Many different analytical models have been developed over the last 40 years that take into account the different physical phenomena involved in contact heat transfer. What follows is not a complete survey of these models, but a look at some that can be of practical use in spacecraft thermal design.

Unfortunately, no universal model exists that can enable one to predict the joint resistance between any two surfaces. To determine which of the available analytical models is appropriate for a situation, the thermal engineer must assess the surface conditions, addressing questions such as: Are the surfaces flat and/or rough? Are oxides on the surfaces? What is the pressure distribution within the contact? What is the real contact area? For surfaces where these questions can be answered with a high degree of certainty, some of the analytical models validated by extensive lab tests can be reliably used to predict overall thermal joint resistance.

In situations where values of the parameters required by the contact-resistance models are not well known, the designer might guess about the surface conditions and select a model to use, or try more than one model to get a feeling for the range of thermal behavior that a particular joint might exhibit. In these situations, however, spacecraft thermal engineers more commonly choose approximate contact-resistance values that have been used successfully in past design efforts. Such generic design values and their use in the thermal-design process are addressed in Chapters 8 and 15. When none of the available models or approximate design values fit the engineer's needs, experimentation is the best choice.

In the material that follows, a list of the parameters influencing thermal contact resistance is presented, followed by a discussion of the various thermal joint-resistance models. Since a complete joint-resistance model should include a thermal-constriction model, a surface-geometry model, and a surface-deformation model,

*Federal University of Santa Catarina, Florianopolis, Brazil.
†University of Waterloo, Waterloo, Canada.

sections will be devoted to each of those topics. Flat, wavy-smooth, and wavy-rough contacting surfaces are treated, and the relevant models are discussed. The effects of oxides or coatings on the contacting surfaces and thermal-interface filler materials on overall joint resistance are also explored. At the end of each subsection, practical, easy-to-apply, and extensively used correlations are presented along with some experimental data. A typical experimental setup used to generate data for model correlation is also presented.

Contact Heat-Transfer Background

Analysis from the microscopic point of view reveals that all machined surfaces have imperfections or deviations from their idealized geometry. These imperfections are usually categorized according to their roughness and waviness. Roughness is a low-scale imperfection and is the result of tool shape, machining process, casting mold, etc. Waviness is a larger-scale imperfection, a consequence of the heat treatment or vibrations and gaps in a vise or other machining equipment.

Because these surface geometrical imperfections are present, only at a few discrete points do flat surfaces actually touch when two bodies are in contact. As pressure between the bodies increases, the highest surface asperities deform, creating regions where the heat flux can flow by conduction. In the regions where the physical contact is not effective, the heat is transferred by conduction, through the gas that fills the gaps, or by radiation. If the bodies are under vacuum conditions, the heat is transferred through the gaps only by radiation.

The heat flux close to the interface is constricted in the microcontact regions, generating a microconstriction resistance, as shown schematically in Fig. 16.1.

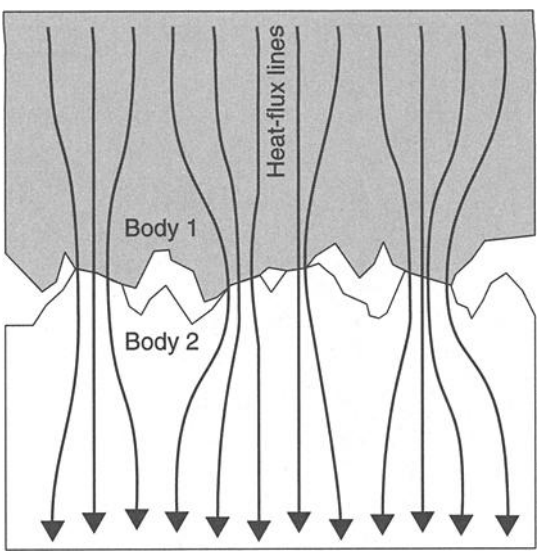

Fig. 16.1. Heat conduction through contacting points (not to scale). (Courtesy F. Milanez)

Macroscopically, the thermal resistance effect can be obtained by measuring the temperature profile of the contacting bodies along their centerline, and extrapolating the resulting one-dimensional line to the contact interface, as illustrated in Fig. 16.2. The contact resistance, R_j, is then defined as the ratio between the temperature drop, T_j, and the heat transferred, or:

$$R_j = \frac{\Delta T_j}{qA_a} \tag{16.1}$$

where q (in W/m^2) is the heat flux that crosses the joint and A_a (in m^2) is the apparent cross-section area.

In the literature, the contact-conductance concept is many times employed instead of the contact-resistance concept and is defined as follows:

$$h_j = \frac{1}{R_j A_a} \tag{16.2}$$

This joint conductance is equal to the sum of three heat conductances in series: the conduction through the contacting points, the radiation through the gaps between the surfaces, and the gas conduction through the gas that fills these gaps, or

$$h_j = h_c + h_r + h_g \tag{16.3}$$

The radiative heat transfer can be modeled as the heat exchange between two gray infinite parallel surfaces, as presented by McWaid.[16.1] For most space applications, this heat-transfer mode can be neglected. Similarly, the gaps between the surfaces are also modeled as two parallel plates separated by a distance equivalent to the average thickness of the gaps. Heat transfer through the gas that fills the gaps is mainly a result of conduction, because the small dimensions of the gaps do not allow convective heat transfer to occur (Song and Yovanovich,[16.2] Hegazy[16.3]). For most space applications, surface contact is in a vacuum environment, and the amount of gas present in the gaps is negligible and so is the conductive

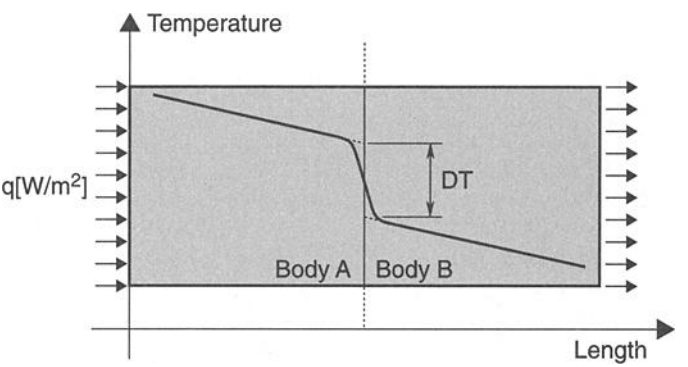

Fig. 16.2. Temperature drop in the joint. (Courtesy F. Milanez)

heat transfer through the gaps. Therefore, for the purpose of discussion in this chapter, the joint conductance is related only to the heat conduction through the contacting points, i.e., $h_j = h_c$.

The contact resistance (or conductance) can be divided into two resistances (or conductances) in series, according to the scale of the surface imperfections. When at least one of the contacting surfaces has large-scale imperfections such as waviness, the contact points are not uniformly distributed over the apparent contact region. They are concentrated in well-defined areas within the apparent contact area. Therefore the heat crossing the interface is first constricted to the macrocontact area (macrocontact resistance) and then through the contact points (microcontact resistance). When both contacting surfaces are specially machined to the point at which they can be considered to be flat, only the microcontact resistance is encountered.

Parameters Influencing Thermal Joint Resistance

Whenever two real surfaces are placed in contact, intimate solid-to-solid contact occurs only at discrete parts of the interface, and the real contact area represents a small fraction (less than 2%) of the nominal contact area. Therefore the pressure at the real contact area is much greater than the apparent contact pressure, and it is related to the flow pressure of the contacting asperity peaks. The interface is idealized as a plane, but the actual thickness of the joint ranges from 0.5 μm for smooth surfaces to about 60 μm for very rough surfaces.

The process of heat transfer across a joint is complex because the thermal resistance can depend upon many geometric, thermal, and mechanical parameters, of which the following are very important.

- geometry of the contacting solids (surface roughness, asperity slope, and waviness)
- gap thickness
- type of interstitial fluid or material (vacuum, grease, foil, etc.)
- thermal conductivities of the contacting solids and the interstitial substance
- hardness or yield pressure of the contacting asperities (which affects the plastic deformation of the highest peaks of the softer solid)
- modulus of elasticity of the contacting solids (which affects the elastic deformation of the wavy parts of the interface)
- average temperature of the interface (which affects material physical properties)

Because thermal contact resistance is such a complex concept, some simplifications are necessary for the development of analytical models and correlations. The following assumptions are made in the development of several contact-resistance models to be discussed later.

- Contacting solids have isotropic thermal and physical properties.
- Contacting solids are thick relative to their surface roughness or waviness.
- Contact is static, so no vibration effect is present.
- Only the first loading cycle is considered, so no hysteresis is present.

- Relative apparent contact pressure (P/H) is neither too small nor too large (between 10^{-6} and 10^{-1}).
- Heat flux is not too large (less than 10^8 W/m^2).

Thermal Joint Resistance Models

As mentioned earlier, a complete contact-resistance model should include a thermal-constriction model, a surface-geometry model, and a surface-deformation model. Several models have been published in the literature covering each of these three main components. Combining these models, one should be able to predict, under some conditions, the thermal contact resistance for the following types of metallic surfaces in contact in a vacuum environment.

- nominally flat, rough surfaces
- smooth wavy surfaces
- rough wavy surfaces

The main objective of this section is not to present a complete survey of the models in the literature; only those considered useful for spacecraft thermal control are discussed here. First, a thermal-constriction model used in most of the thermal contact-resistance studies will be presented, followed by a surface-geometry model and a surface-deformation model. These models are then combined, resulting in complete models that sometimes can be presented in the form of correlations. Before selecting the model to be used in a spacecraft thermal-design calculation, the engineer should analyze the hypotheses adopted in the various models so that the most appropriate model can be applied to the problem.

Thermal-Constriction Models

The conductive heat transfer that occurs through the actual contact points resulting from the physical interaction between two surfaces has been studied extensively in the last four decades. The heat-transfer models developed for this purpose can be divided into two main groups: microconstriction models that are usually used for conforming surfaces and macroconstriction models used for interactions where at least one surface has considerable waviness.

Microconstriction Thermal Resistance Models

Figure 16.3(a) shows a schematic of the points resulting from the contact between two rough, nominally flat surfaces. Cooper *et al.*[16.4] demonstrated that if the surfaces do not have waviness, the contact spots are randomly distributed over the apparent contact area. Furthermore, if the geometry and the thermal properties of the contacting surfaces are isotropic, all the contact points are approximately circular, isothermal, and at about the same temperature level. Under such circumstances, an elemental heat-flux tube can be associated with each contact spot, as shown in Fig. 16.3(b).

The elemental heat-flux tube, of radius b, defines the influence region of the contact spot, of radius a, located at its center. Far from the interface, the heat-flux lines are considered parallel, and they converge to the contact spot as the heat flux approaches the interface. The temperature distribution within the tube, of conductivity k_1, is axisymmetric. The following boundary conditions are applied:

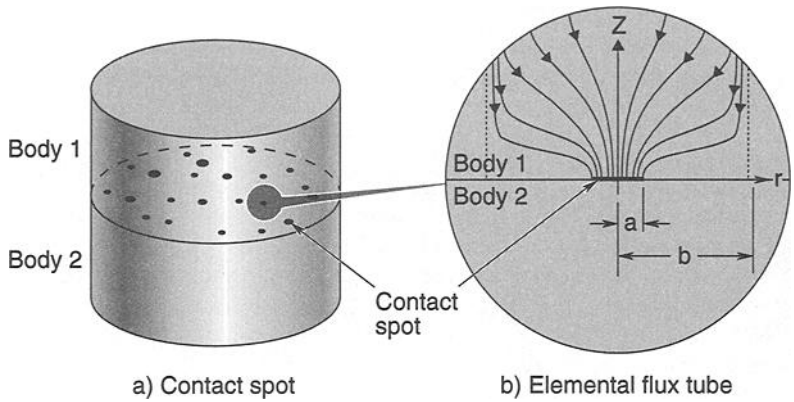

Fig. 16.3. ***(Fig. 8.6, reproduced here for your convenience.)*** **Microcontacts and constricted heat flow.** (Courtesy F. Milanez)

$$\left.\begin{aligned} T &= T_0 = \text{constant} && 0 \le r < a \\ k_1 \frac{\partial T}{\partial z} &= 0 && a < r < b \end{aligned}\right\} \quad \text{at} \quad z = 0 \tag{16.4}$$

$$k_1 \frac{\partial T}{\partial z} \to \frac{Q}{\pi b^2} \qquad z \to \infty \tag{16.5}$$

$$k_1 \frac{\partial T}{\partial r} = 0 \qquad r = b \tag{16.6}$$

The main difficulty in solving this problem is the mixed boundary condition at $z = 0$. Many different approaches were employed to obtain the analytical solution, and different expressions were obtained. These solutions actually led to similar temperature-distribution results, as presented by Mikic and Rohsenow.[16.5] Based on this work, Cooper *et al.*[16.4] proposed the substitution of the isothermal contact at $0 < r < a$ by a heat-flux condition, where the resulting temperature distribution is nearly constant over that area. This new condition is:

$$\left.\begin{aligned} k_1 \frac{\partial T}{\partial z} &= \frac{Q}{2\pi a \sqrt{a^2 - r^2}} && 0 < r < a \\ k_1 \frac{\partial T}{\partial z} &= 0 && a < r < b \end{aligned}\right\} \quad \text{at} \quad z = 0 \tag{16.7}$$

The resulting expression for the microconstriction resistance for the heat-flux tube is:

$$R_s = \frac{\psi}{4k_1 a} \tag{16.8}$$

where the constriction parameter ψ can be approximated by the following expression, valid for $0 < a/b < 0.4$:

$$\psi = \left[1 - \left(\frac{a}{b}\right)\right]^{1.5} \tag{16.9}$$

Adding in series the microconstriction resistances of the two elemental tubes that form the contact, one gets the contact resistance of the ith contact spot:

$$R_{si} = \frac{\left(1 - \frac{a_i}{b_i}\right)^{1.5}}{4k_1 a_i} + \frac{\left(1 - \frac{a_i}{b_i}\right)^{1.5}}{4k_2 a_i} \tag{16.10}$$

The contact resistance is the sum of the microconstriction resistances of N contact spots in parallel. It is given by:

$$\frac{1}{R_c} = 2k_s \sum_{i=1}^{N} \frac{a_i}{\left(1 - \frac{a_i}{b_i}\right)^{1.5}} \tag{16.11}$$

where $k_s = \frac{2k_1 k_2}{k_1 + k_2}$ is the harmonic mean of the conductivities of the two bodies (1 and 2) in contact.

The challenge now is to quantify the number and size of the contact spots and the radius of the elemental heat-flux tubes. The problem is simplified if the contact radius a_i and the tube radius b_i are approximated by their mean values a and b. Actually, the ratio $\frac{a}{b}$ can be expressed as a function of the ratio between the real contact area, A_r, and the apparent contact area, A_a, by the expression (Yovanovich, 1982):

$$\frac{a}{b} = \sqrt{\frac{A_r}{A_a}} \tag{16.12}$$

For N contact spots, the contact resistance can be expressed as

$$R_c = \frac{1}{\sum_{i=1}^{N} \frac{1}{R_{si}}} = \frac{\psi}{2k_s a N} \tag{16.13}$$

and the contact conductance as

$$h_c = \frac{1}{A_a R_c} = \frac{2k_s}{A_a} \frac{Na}{\left(1 - \sqrt{\frac{A_r}{A_a}}\right)^{1.5}} = 2k_s \frac{na}{\left(1 - \sqrt{\frac{A_r}{A_a}}\right)^{1.5}} \tag{16.14}$$

where $n = \frac{N}{A_a}$ is the contact-spot density per unit apparent area.

In a study based on the Roess[16.6] analysis, Clausing and Chao[16.7] obtained an expression similar to Eq. (16.13) for determining the microconstriction resistance. They used a different constriction parameter, ψ, given by:

$$\psi\left(\frac{a}{b}\right) = 1 - 1.40925\left(\frac{a}{b}\right) + 0.29591\left(\frac{a}{b}\right)^3 + 0.05254\left(\frac{a}{b}\right)^5 + 0.02105\left(\frac{a}{b}\right)^7 + \ldots \tag{16.15}$$

This ψ expression is in close agreement to the results of Eq. (16.9) for $0 < a/b < 0.4$ and differs by a few percent for $a/b = 0.6$.

Macroconstriction Thermal Resistance Models

Clausing[16.8] observed that flat surfaces are difficult to produce. As a result of the fabrication process, many surfaces have waviness, and when they are put into contact, the actual microcontact spots are concentrated in well-defined regions. Therefore, the heat flux crossing the joint experiences two constrictions: the micro, as described in the last section, and the macro, where the heat-flux lines are constricted to the region where the contact spots are located. Clausing considered the thermal contact resistance as composed of three resistances in series: macroconstriction, microconstriction, and oxide-film resistance. Clausing and Chao[16.7] modeled the surface waviness by means of spherical crowns on the tops of cylinders. The macroscopic contact area was determined by means of the Hertz elastic theory for two spherical surfaces subjected to a mechanical load. The microcontact spots were considered uniformly distributed over the macrocontact areas.

Figure 16.4 shows a schematic of the apparent contact region between two cylinders of identical radius b_L. The waviness of the contacting surfaces is represented by spherical crowns of radius r_1 and r_2. The distances d_1 and d_2 represent the waviness height. For determining the macrocontact resistance, Clausing and Chao[16.7] assumed that:

- the length of the cylinder is large in comparison to b_L
- the contact is perfect over the macrocontact area
- the heat is transferred only by conduction across the macrocontact area
- the cylinder temperature is uniform far from the contact plane
- the material properties of the contacting solids are isotropic, homogeneous, and constant with temperature
- $d_i << r_i$ ($i = 1$ and 2).

The macroconstriction and microconstriction resistance problems are very similar, and the left side of Fig. 16.4 is also representative of the microconstriction resistance. The actual contact spots are considered uniformly distributed inside the contour area, according to the surface waviness. Therefore Eqs. (16.13) and (16.15)

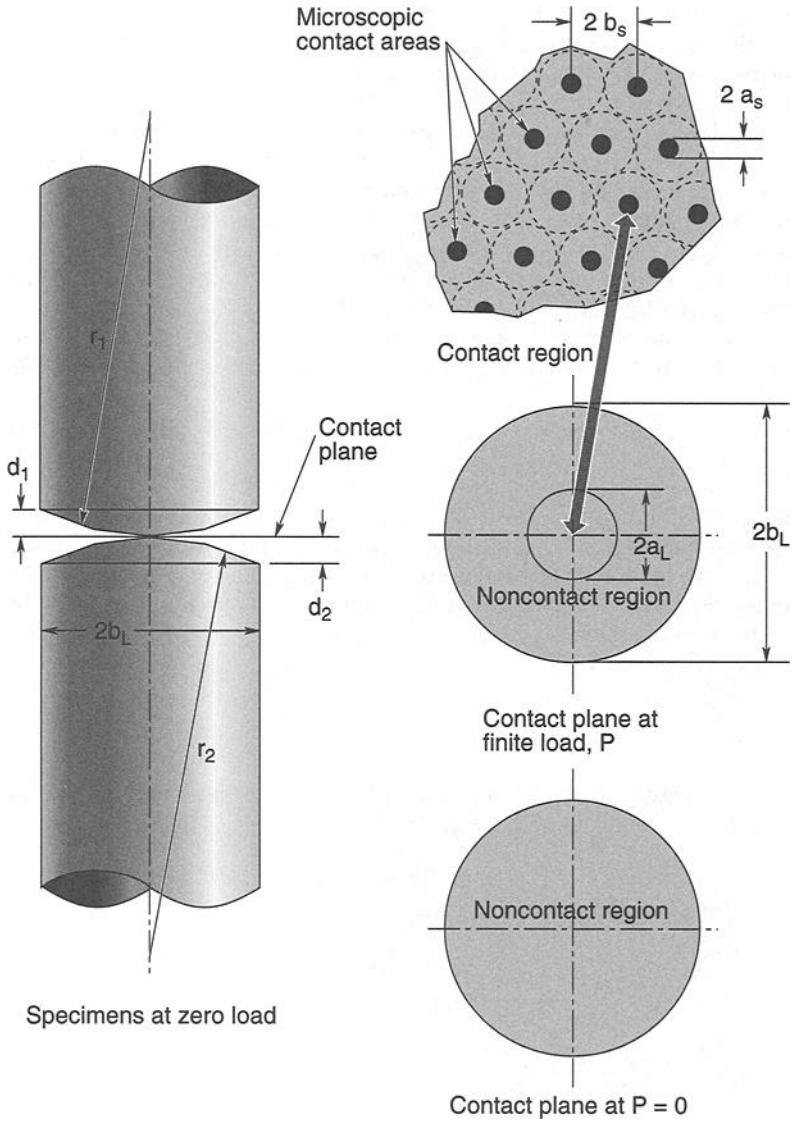

Fig. 16.4. ***(Fig. 8.7, reproduced here for your convenience.)*** **Schematic of the apparent contact area, according to Clausing and Chao.[16.7]**

can be applied to determine the macroconstriction resistance, where a/b is replaced by a_L/b_L. In the next section, a model to determine a_L/b_L, the ratio of the apparent contact-area radius to the cylinder radius, will be discussed. The model of Clausing and Chao[16.7] is applicable when the flatness deviation is several times greater than the roughness. Actually, the Hertz theory was developed for smooth

spherical contacting surfaces, and a correction factor should be applied because the roughness increases the contact area. Clausing and Chao[16.7] did not account for the roughness effect, which is negligible for very wavy surfaces.

Mikic and Rohsenow[16.5] developed a mathematical model for a physical model similar to the mathematical model developed by Clausing and Chao. The expression they obtained is similar. They also concluded that the macro- and microconstriction resistances are similar phenomena that can be described by the same analytical formulation, if the appropriate characteristic dimensions are used. The macrocontact area is estimated using the Hertz theory. Again, Eq. (16.13) can be used for calculation of the macroscopic thermal contact resistance, R_L, with the ψ parameter given by Eq. (16.9), where a/b is replaced by a_L/b_L or D/L, where D represents the diameter of the contour area, L is the wavelength of the spherical waviness (Fig. 16.5), and $N = 1$. This results in the following expression, valid for $0 < D/L < 0.4$:

$$R_L = \frac{\psi}{2k_s a_L} = \frac{\psi}{k_s D} \tag{16.16}$$

Mikic and Rohsenow[16.5] also conducted analytical studies of the heat flow through the macroscopic heat channel, where the contour area is in the form of a strip. This geometry may appear as a result of some machining process. When the contour area is kept at a constant temperature, the constriction resistance of one half of the heat channel is:

$$R_L = \frac{1}{k\pi^2}\frac{b}{a}\sum_{i=1}^{\infty}\frac{1}{i^2}J_0\left(i\pi\frac{a}{b}\right)\sin\left(i\pi\frac{a}{b}\right) \tag{16.17}$$

When the heat flux over the contour area is taken to be uniform, the constriction resistance can be expressed as in Eq. (16.18).

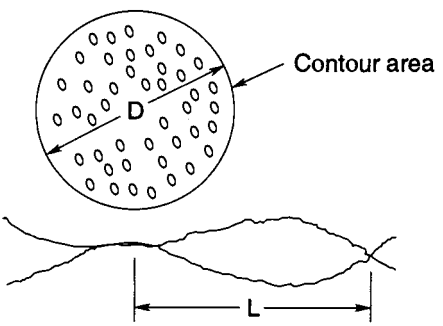

Fig. 16.5. Schematic of rough wavy contacting surfaces. (Mikic and Rohsenow[16.5])

$$R_L = \frac{1}{k\pi^3}\left(\frac{b}{a}\right)^2 \sum_{i=1}^{\infty} \frac{1}{i^3} \sin^2\left(i\pi\frac{a}{b}\right) \tag{16.18}$$

In the last two equations, a represents the half width of the strip and b the half width of the macroscopic heat channel (see Fig. 16.6a).

Mikic and Rohsenow[16.5] also developed the macroconstriction resistance of two surfaces in contact where the contour area forms a rectangle. For the case of a uniform heat flux over the contour area, the constriction resistance is

$$R_L = \frac{4bc}{k_s\pi^3}\left[\frac{b^2}{ca^2}\sum_{i=1}^{\infty}\frac{\sin\left(\frac{i\pi a}{b}\right)}{i^3} + \frac{c^2}{bd^2}\sum_{j=1}^{\infty}\frac{\sin^2\left(\frac{j\pi d}{c}\right)}{j^3}\right] \tag{16.19}$$

$$+\frac{8b^2c^2}{k_s\pi^2a^2d^2}\sum_{i=1}^{\infty}\sum_{j=1}^{\infty}\frac{\sin^2\left(\frac{i\pi a}{b}\right)\sin^2\left(\frac{j\pi d}{c}\right)}{i^2j^2\sqrt{\left(\frac{i\pi}{b}\right)^2+\left(\frac{j\pi}{c}\right)^2}}$$

where a, b, c, and d are as shown in Fig. 16.6b.

Macro/Microcontact Thermal Resistance Models

When heat crosses an interface between two contacting surfaces, the flow is first constricted to the large-scale contact areas, and then it is further constricted to the microscopic contact spots within this macroscopic area. The thermal contact resistance of this joint, in the absence of a conducting fluid, can be represented by two resistances in series: the large-scale or macroscopic resistance, R_L, and the small-scale or microscopic resistance, R_s:

$$R_c = R_s + R_L \tag{16.20}$$

Substituting the appropriate expressions for R_L and R_s, one gets an analytical model that takes into account both the macro- and microcontact resistances. According to Clausing and Chao,[16.7] Yovanovich,[16.9] and Mikic and Rohsenow,[16.5] this resistance can be determined by:

$$R_c = \frac{\psi\left(\frac{a}{b}\right)}{2k_saN} + \frac{\psi\left(\frac{D}{L}\right)}{k_sD} \tag{16.21}$$

where the parameter D/L may be replaced by D_{eff}/L, to account for the influence of the roughness over the contacting area, using the model developed by Mikic and Rohsenow,[16.5] which will be presented in the next section.

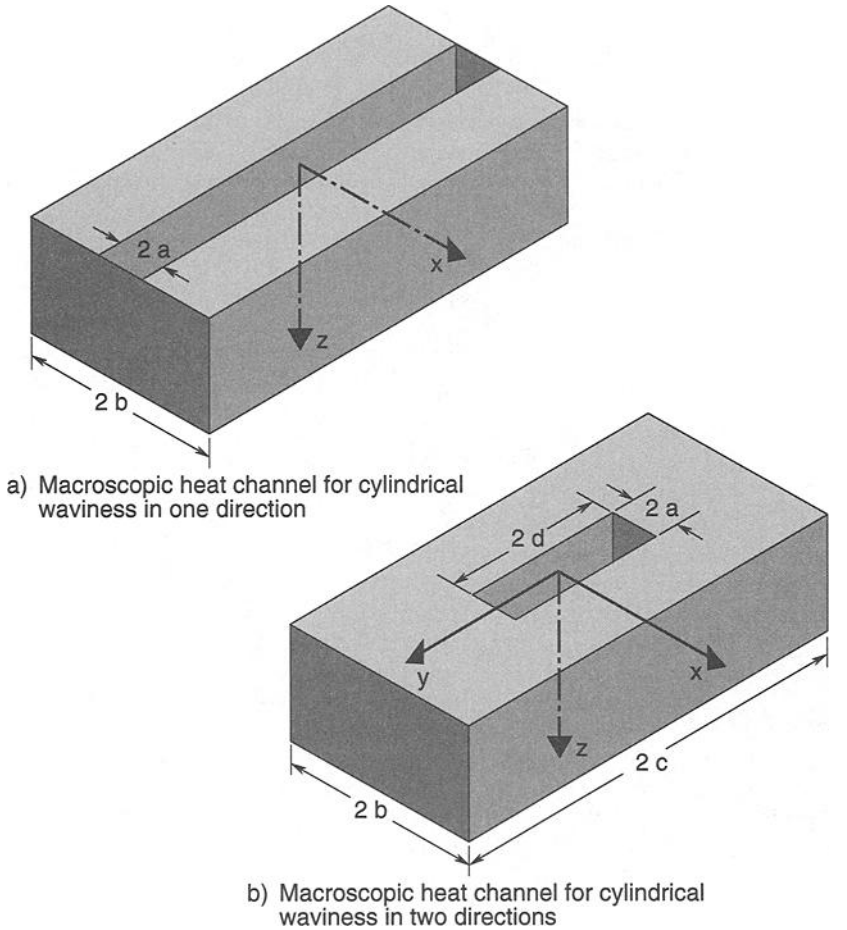

Fig. 16.6. Special macroscopic heat channels. (Mikic and Rohsenow[16.5])

An alternative expression for overall thermal contact resistance is presented by Mikic and Rohsenow:[16.5]

$$R_c A_a = \frac{1}{h_c} = \frac{\psi\left(\frac{a}{b}\right)}{2k_s\left(\frac{a}{b}\right)\sqrt{\frac{n}{\pi}}} + \frac{\psi\left(\frac{D}{L}\right)}{\frac{4}{\pi}k_s\left(\frac{D}{L}\right)}L \tag{16.22}$$

One should note in this case that n is obtained from the macrocontact area

$$A_L = N_L\frac{\pi D^2}{4} = n\pi b^2 \tag{16.23}$$

where:

$$N_L = \frac{A_a}{\pi \frac{L^2}{4}} \tag{16.24}$$

Then, the number of microcontacts per unit apparent area is

$$n = \frac{\left(\frac{D}{L}\right)^2}{\pi b^2} \tag{16.25}$$

Again, in Eqs. (16.22) and (16.25) D/L may be replaced by D_{eff}/L.

Other studies in macro/microcontact thermal resistance can be found in the literature. Burde and Yovanovich[16.10] studied the theoretical thermal resistance of rough wavy contacts. They considered a contact between a flat rough surface and a smooth sphere. The equivalent roughness of the contacting surfaces is considered concentrated on the flat surface and the equivalent waviness on the sphere. The authors obtained an expression for the contact resistance, but their results were only compared with data obtained from idealized smooth spherical/rough flat contacts. Lambert and Fletcher[16.11] (1997) also studied the thermal contact resistance of spherical rough metals. They considered that the pressure within the contacting surfaces is not uniform and used an expression, developed by Mikic,[16.12] to represent the pressure as a function of the radius. They showed that their model is in good agreement with the literature data, but they did not obtain an analytical expression for the thermal resistance.

Geometric and Deformation Models for Flat Rough Surfaces

The thermal-constriction models presented above demonstrate that the number of contacts per unit of contour area and the ratio between the apparent area and real contact area are important parameters. The ratio A_r/A_a is expected to be very small when conforming flat rough surfaces are in contact under typical pressures, and therefore the mean pressure applied in the real contact area is much higher than the nominal applied pressure. The question that arises is whether the behavior of the contacting asperities, subjected to this high stress, is elastic or plastic. Cooper *et al.*[16.4](1969) state that if the surfaces are imagined to be moving normally toward each other under increasing pressure, successive contacts are made, which are deformed elastically and then may flow plastically as the nominal interface pressure increases.

A critical review of the elastic and plastic thermal contact resistance models available in the literature is presented by Sridhar and Yovanovich,[16.13] who compared several plastic models and concluded that they generally present the same trends and results. Because the model developed by Cooper *et al.*[16.4] requires fewer parameters, they selected this model. A similar study was conducted for elastic deformation, and Mikic's[16.14] model was selected. Sridhar[16.15] also developed an elastoplastic model, which takes into account both the elastic and plastic deformation of the asperities. In this section, these three models are briefly described.

Plastic-Deformation Model

Independent studies by Mikic *et al.*[16.16] and Greenwood and Williamson[16.17] assumed that the asperities can be represented by spherical surfaces in contact and that the heights of the asperities on the surfaces form a Gaussian distribution. They suggested that even at moderate nominal pressures, very few contact points are each subjected to only light pressure, so the asperities are deformed elastically.

Mikic *et al.*,[16.16] Cooper *et al.*,[16.4] and Yovanovich[16.18] employed a Hertzian elastic analysis to determine the stresses as a function of the interference and deduce the interference at which elastic stress is exceeded and behavior becomes plastic. They assumed that the contacts are all plastic and that, at each contact, the pressure is equal to the maximum that can be sustained by the softer of the two materials when plastically deformed.

Each surface in contact can be characterized by several sample profiles taken from the surface, from which statistical properties can be deduced. The surface profile $y(x)$, illustrated in Fig. 16.7, can be considered a random stationary process, meaning that the group of profiles is invariant. Furthermore, the probability density of height and slope are assumed to be independent, and the surface height is assumed to be normally distributed, with the probability density function

$$p(y)=\frac{e^{-\frac{y^2}{2\sigma^2}}}{\sigma\sqrt{2\pi}} \tag{16.26}$$

where σ represents the standard deviation for height (or root mean square deviation), specified by the relation

$$\sigma=\left[\frac{1}{L}\int_0^L y^2 dx\right]^{1/2}=\left[\int_{-\infty}^{\infty} y^2 p(y)\,dy\right]^{1/2} \tag{16.27}$$

and readily obtained from the profilometer.

In analysis of the geometry, the conforming surface contact is modeled as the interaction between two surfaces—a rough, rigid, nominally flat surface, which is pressed against the other one, a perfectly flat and smooth surface that is Y distance away from the mean plane of the rough surface. As the surfaces are pressed

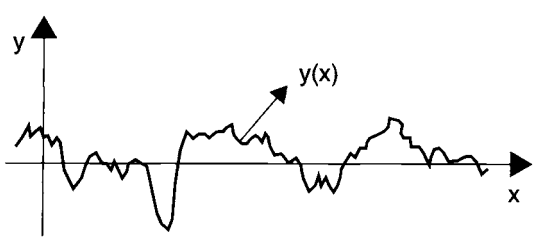

Fig. 16.7. Contacting surface profile. (Courtesy F. Milanez)

against each other, the asperity peaks penetrate into the smooth surface, which experiences a plastic deformation. This physical model is represented schematically in Fig. 16.8. The details of this geometric analysis are described by Mikic[16.5,16.14,16.19] and by Cooper *et al.*[16.4] These hypotheses lead the problem to a geometric analysis of the interference lengths, which are converted to areas, yielding the following important results.

The contact conductance parameter:

$$\frac{1}{A_a}\sum_{i=1}^{N} a_i = \frac{1}{4\sqrt{2\pi}}\frac{m}{\sigma}e^{-x^2} \tag{16.28}$$

The relative real contact area:

$$\varepsilon^2 = \frac{A_r}{A_a} = \left(\frac{a}{b}\right)^2 = \frac{1}{2}erfc(x) \tag{16.29}$$

The contact-spot density:

$$n = \frac{1}{16}\left(\frac{m}{\sigma}\right)^2 \frac{e^{-2x^2}}{erfc(x)} \tag{16.30}$$

The mean contact-spot radius

$$a = \sqrt{\frac{8}{\pi}}\frac{\sigma}{m}e^{x^2}erfc(x) \tag{16.31}$$

where $x = \frac{Y}{\sqrt{2}\sigma}$ and $\frac{Y}{\sigma}$ is called the relative mean plane separation. The surface parameter m is the effective absolute surface slope.

The hypothesis adopted when two rough surfaces are in contact is exactly the same as the one presented in Fig. 16.8, i.e., that a rough, rigid surface, with equivalent roughness and slope, penetrates a perfectly flat and smooth surface. Equations

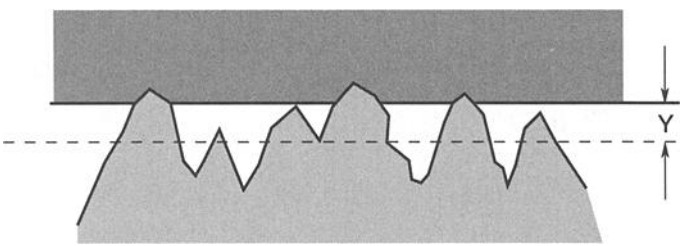

Fig. 16.8. Asperities-deformation model of a rough, rigid, nominally flat surface pressed against a smooth flat surface, *Y* distance away from the mean plane of the rough surface. (Courtesy F. Milanez)

(16.28) to (16.31) are valid, with the mean planes considered Y distance apart and with the roughness and slope given by

$$\sigma^2 = \sigma_1^2 + \sigma_2^2 \tag{16.32}$$

and

$$m^2 = m_1^2 + m_2^2 \tag{16.33}$$

where the indexes 1 and 2 refer to the contacting surfaces.

An important observation is that the only parameter left is the macrocontact area, whose determination is not made by means of a statistical treatment of the surfaces, but through a deformation analysis.

Yovanovich[16.18] proposed a correlation, which compared within ±1.5% with the complete theory, including the thermal, geometric, and deformation aspects, for $2 \le \frac{Y}{\sigma} \le 4.75$:

$$\frac{h_c \sigma}{k_s m} = 1.25\left(\frac{P}{H_c}\right)^{0.95} \tag{16.34}$$

Hegazy[16.3] observed that the surface microhardness H_c is not constant with depth. The regions close to the surface are harder as a result of the work-hardening process. He proposed a method for determining the appropriate contact hardness, based on the Vickers microhardness measurement. This method was improved by Song and Yovanovich,[16.2] who proposed the following expression for the nondimensional contact pressure, where C_1 and C_2 are the Vickers correlation coefficients, given in Table 16.1, and σ/m is given in μm.

$$\frac{P}{H_c} = \left\{ P / \left[C_1 \left(1.62 \frac{\sigma}{m} \right) \right]^{C_2} \right\}^{\frac{1}{1 + 0.071 C_2}} \tag{16.35}$$

This expression can be inserted in Eq. (16.34) for any level of contacting pressure, improving the precision of the results.

Table 16.1. Vickers Microhardness Parameters (Hegazy[16.3])

Material	C_1 (MPa)	C_2
Ni 200	6.3	-0.264
SS 304	6.27	-0.229
Zr-Nb	5.88	-0.267
Zr-4	5.677	-0.278
Al-6061	1.11	-0.00487[a]

[a]Nho [16.21]

The experimental data obtained by Hegazy[16.3] provide ample evidence that the preceding conforming rough-surface contact-conductance model is accurate. Data were obtained under vacuum conditions for a variety of metals, including SS 304, Zr - 4, and Ni 200. Each interface consisted of a relatively smooth, lapped surface and a rough, bead-blasted surface of identical material. The surface roughness parameter σ/m was 8.2 μm to 12.4 μm for the smoothest interfaces and 38.3 μm to 59.8 μm for the very rough interfaces. The mean interface temperature ranged from 99°C to 178°C. For apparent contact pressures ranging between approximately 0.45 MPa to 890 MPa, the measured contact conductance obtained by the Eq. (16.34) correlation, where $\frac{P}{H_c}$ is determined by Eq. (16.35), shows very good agreement with data. In the plot shown in Fig. 16.9, the dimensionless contact conductance is shown as a function of the dimensionless contact pressure, and the correlation and data are compared.

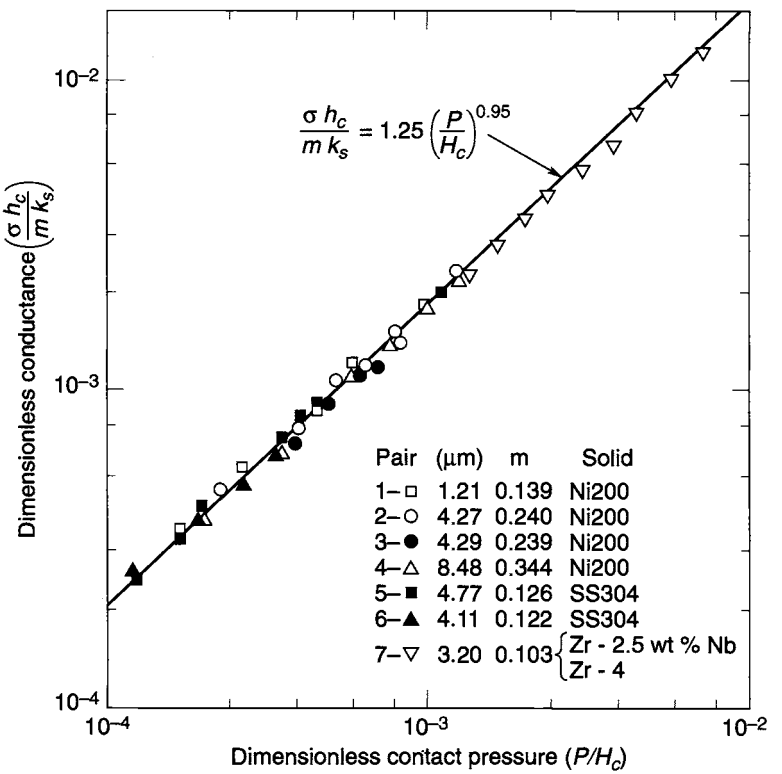

Fig. 16.9. Comparison of contact-conductance theory against test data for clean, bare surfaces in vacuum.

Elastic-Deformation Model

Mikic[16.14] derived an expression for an asperity in contact with a flat surface in elastic deformation. The asperity is considered to be hemispherical, and the contact area is related to the displacement using Hertzian theory. Mikic showed that, at the same separation of the mean contacting planes Y, the contact area for purely plastic deformation for any specific asperity is twice the contact area in elastic deformation, or:

$$\frac{A_{r,\,\text{elastic}}}{A_{r,\,\text{plastic}}} = \frac{1}{2} \tag{16.36}$$

Therefore, using the expressions obtained for plastic-deformation contacts, one obtains the following expressions.

Contact conductance parameter:

$$\frac{1}{A_a}\sum_{i=1}^{N} a_i = \frac{1}{8\sqrt{\pi}}\frac{m}{\sigma}e^{-x^2} \tag{16.37}$$

Relative real contact area:

$$\varepsilon^2 = \frac{A_{r_{\text{elastic}}}}{A_a} = \frac{1}{4}erfc(x) \tag{16.38}$$

Contact-spot density (same as plastic deformation):

$$n = \frac{1}{16}\left(\frac{m}{\sigma}\right)^2 \frac{e^{-2x^2}}{erfc(x)} \tag{16.39}$$

Mean contact-spot radius:

$$a = \frac{2}{\sqrt{\pi}}\frac{\sigma}{m}e^{x^2}erfc(x) \tag{16.40}$$

Mikic[16.14] derived an expression for the ratio of real to apparent area for two isotropic rough surfaces undergoing elastic deformation:

$$\frac{A_r}{A_a} = \frac{\sqrt{2}P}{E'm} \tag{16.41}$$

where

$$E' = \frac{E_1 E_2}{E_2(1-\nu_1^2) + E_1(1-\nu_2^2)} \tag{16.42}$$

and where E is modulus of elasticity, ν is Poisson's ratio, and m is given by Eq. (16.33).

This theory was correlated through the relation

$$\frac{h_c \sigma}{k_s m} = 1.55\left(\frac{P\sqrt{2}}{E' m}\right)^{0.94} \tag{16.43}$$

Mikic[16.14] observed that h_c is a very weak function of m. Taking $m = 0.1$, which is the average value for blasted surfaces, one gets the following expression, which can be used for most metallic contacts under elastic deformation:

$$h_{se} = 1.9\frac{k}{\sigma}\left(\frac{P}{E'}\right)^{0.94} \tag{16.44}$$

Sridhar and Yovanovich Elastoplastic Deformation Model

Sridhar and Yovanovich[16.20] developed a single deformation model for asperities of a flat rough surface experiencing partially elastic and partially plastic deformation. They combined the plastic model of Cooper *et al.*[16.4] (1969) and the elastic models of Mikic[16.14] and concluded that the ratio of the actual to the apparent area is equivalent to the ratio of the contact pressure to the elastoplastic hardness H_{ep} of the material. That is:

$$\frac{A_r}{A_a} = \frac{P}{H_{ep}} \tag{16.45}$$

They also obtained the following expressions.

Contact conductance parameter:

$$\frac{1}{A_a}\sum_{i=1}^{N} a_i = \frac{1}{4\sqrt{2\pi}}\frac{m}{\sigma}e^{-x^2}\sqrt{f_{ep}} \tag{16.46}$$

Relative real contact area:

$$\varepsilon^2 = \frac{A_r}{A_a} = \left(\frac{a}{b}\right)^2 = \frac{f_{ep}}{2}erfc(x) \tag{16.47}$$

Contact-spot density:

$$n = \frac{1}{16}\left(\frac{m}{\sigma}\right)^2 \frac{e^{-2x^2}}{erfc(x)} \tag{16.48}$$

Mean contact-spot radius:

$$a = \sqrt{\frac{8}{\pi}}\sqrt{f_{ep}}\frac{\sigma}{m}e^{x^2}erfc(x) \tag{16.49}$$

where f_{ep} is obtained by the expression

$$f_{ep} = \frac{\left\{1 + \left[6.5/\left(4.61\sqrt{\left(\frac{E'm}{H_{ep}}\right)^2 - 2}\right)\right]^2\right\}^{1/2}}{\left\{1 + \left[13/\left(4.61\sqrt{\left(\frac{E'm}{H_{ep}}\right)^2 - 2}\right)\right]^{1.2}\right\}^{1/1.2}} \tag{16.50}$$

and the nondimensional contact pressure is obtained by

$$\frac{P}{H_{ep}} = \left[\frac{0.9272P}{C_1\left(1.62\frac{\sigma}{m}f_{ep}^{0.429}\right)^{C_2}}\right]^{\frac{1}{1+0.071C_2}} \tag{16.51}$$

The microhardness parameters C_1 and C_2, presented in Table 16.1, were obtained by Hegazy[16.3] and Nho,[16.21] for conforming rough surfaces. To determine P/H_{ep}, one must use an iterative procedure involving Eqs. (16.50) and (16.51).

With the objective of getting a correlation for their elastoplastic model, Sridhar and Yovanovich[16.20] proposed an index η, given by

$$\eta = 1.67\frac{E'}{S_f}m \tag{16.52}$$

where S_f is the material yield or flow stress, given by

$$S_f = \frac{1}{2.76\sqrt{\frac{1}{H_{ep}^2} - \frac{2}{(E'm)^2}}} \tag{16.53}$$

which specifies whether the asperities deformation is elastic ($0 < \eta < 5$), plastic ($400 < \eta < \infty$), or elastoplastic ($5 < \eta < 400$). For the elastic regime, their model reduces to the Mikic[16.14] correlation, which is given by Eq. (16.43). For the plastic regime, their model reduces to the Yovanovich plastic correlation, given by Eq. (16.34) with Eq. (16.35). For the elastoplastic regime, they proposed the following correlation:

$$\frac{h_{sep}}{k}\frac{\sigma}{m} = 1.245\left(1 + \frac{46690.2}{\eta^{2.48}}\right)^{1/30}\left(\frac{P}{H_{ep}}\right)^{0.948\left[1/\left(1+\frac{2086.9}{\eta^{1.842}}\right)\right]^{1/600}} \tag{16.54}$$

Equation (16.54) together with Eqs. (16.52), (16.53), (16.49), and (16.50) constitute the Sridhar and Yovanovich elastoplastic model. Its evaluation requires an iterative process, but the convergence is fast, because f_{ep} varies between 0.5 and 1.

Sridhar[16.15] used data from Hegazy[16.3] and Antonetti[16.22] in addition to his own to compare with his elastoplastic model, covering a wide range of thermal, material, and surface properties. The pressure ranged from 0.4 MPa to 8.9 MPa. The elastic modulus varied from 96 GPa for the zirconium alloys to 207 MPa for the

Ni 200 and SS 304. The data also covered a wide range of surface roughness (6 $\mu m < \sigma/m < 60\ \mu m$), mean interface temperatures ($108 < T_c < 175°C$), and thermal properties ($10 < k_s < 77$ W/m·K). Figure 16.10 shows good agreement of all data with the two theoretical extremes, using the elastoplastic model: a full plastic and a full elastic asperity deformation. All the experimental data are expected to be within these two extreme curves.

Geometric and Deformation Models for Wavy Smooth Surfaces

Clausing and Chao[16.7] and Mikic and Rohsenow[16.5] modeled waviness as spherical caps of radii r_1 and r_2, as shown in Figs. 16.2 and 16.3. They assumed that the waviness is not too pronounced, i.e., $d/L << 1$. For the determination of the macrocontact area, they assumed that a perfect contact exists over the macroscopic contact area, i.e., $R_s << R_L$. They considered the deformation to be elastic and used the same Hertzian solution as before for the contact area of two spheres. The radius of the macrocontact area a_L is

$$a_L = \left[\frac{3P}{4}\left(\frac{1-\nu_1^2}{E_1}+\frac{1-\nu_2^2}{E_2}\right)\left(\frac{1}{r_1}+\frac{1}{r_2}\right)^{-1}\right]^{1/3} \tag{16.55}$$

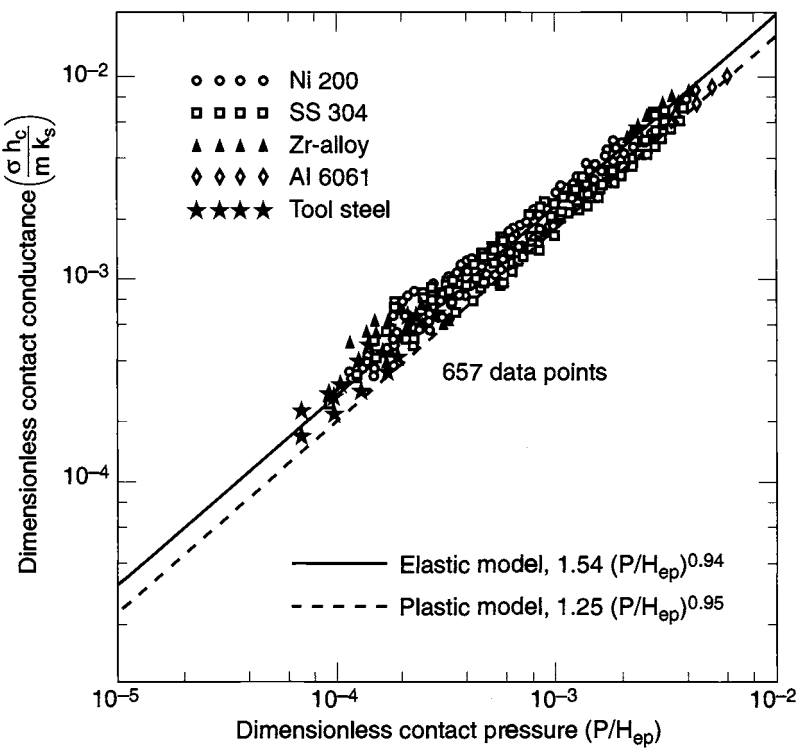

Fig. 16.10. Comparison of data with the elastoplastic model.

For most metals, where $\nu_1^2 = \nu_2^2 = (0.01)^2$, the ratio a_L/b_L, which is equivalent to the ratio of the macrocontact area diameter to the length of the waviness (D/L) (see Fig. 16.3), is shown to be

$$\frac{a_L}{b_L} = \frac{D}{L} = 1.285\left[\left(\frac{P_a}{E_s}\right)\left(\frac{b_L}{d_t}\right)\right]^{1/3} \tag{16.56}$$

where $d_t = d_1 + d_2$ and $E_s = \dfrac{2E_1E_2}{E_1 + E_2}$ is the harmonic mean of the moduli of elasticity for the materials in contact.

Geometric and Deformation Models for Wavy Rough Surfaces in Contact

If the wavy surface in contact is also rough, one can anticipate that the contour area is larger than what is predicted by the Hertz theory and that the density of the contacting spots is not uniformly distributed, but decreases as the radius increases. Mikic[16.5] assumed a uniform distribution inside the contour area and obtained the following expression for the effective contact area, assuming that the mean surface deforms elastically:

$$\lambda_{\text{eff}} = \lambda^2 + 2\int_{\lambda}^{1} \exp\left\{-\frac{d_t}{\sigma}\lambda^2 g\left(\frac{\lambda}{\lambda_H}\right)\left[2\sqrt{2}x + \frac{d_t}{\sigma}\lambda_H^2 g\left(\frac{\lambda}{\lambda_H}\right)\right]\right\}\lambda\, d\lambda \tag{16.57}$$

where $\lambda_{\text{eff}} = \dfrac{D_{\text{eff}}}{L}$, $\lambda_H = \dfrac{D}{L}$, $\lambda = \dfrac{2r}{L}$, r is the contact radius axis, and $g\left(\dfrac{\lambda}{\lambda_H}\right)$ is

$$g\left(\frac{\lambda}{\lambda_H}\right) = \left(\frac{\lambda}{\lambda_H}\right)^2 - 2\left\{1 - \frac{1}{\pi}\left[\left(2 - \frac{\lambda^2}{\lambda_H^2}\right)\sin^{-1}\left(\frac{\lambda}{\lambda_H}\right) + \left(\frac{\lambda^2}{\lambda_H^2} - 1\right)^{1/2}\right]\right\} \tag{16.58}$$

The parameter that appears in Eqs. (16.29), (16.38), or (16.47) is a function of λ, where

$$\varepsilon = \frac{1}{\lambda_{\text{eff}}}\left(\frac{P}{H}\right)^{1/2} \tag{16.59}$$

Obviously λ_{eff} is determined through an iterative process involving Eqs. (16.57) and (16.58), one that is expected to converge very quickly.

Clausing and Chao,[16.7] considering the contact resistance as consisting of the macro- and the microresistances in series, obtained the following correlations for the macro- and microconductances respectively:

$$h_L = \frac{k_s}{b_L}\frac{2 \cdot 1.285\left[\left(\dfrac{P_a}{E_s}\right)\left(\dfrac{b_L}{d_t}\right)\right]^{1/3}}{\pi\psi\left\{1.285\left[\left(\dfrac{P_a}{E_s}\right)\left(\dfrac{b_L}{d_t}\right)\right]^{1/3}\right\}}, \text{ for } \frac{a_L}{b_L} < 0.65 \tag{16.60}$$

$$h_c = \frac{2P_a k_s}{\pi \xi H a \psi\left(\frac{a}{b}\right)} \tag{16.61}$$

where the factor ξ was suggested by Holm[16.23] to account for the elastic deformation of the asperities that is often assumed to be unity (plastic deformation). Figure 16.11, from Clausing and Chao,[16.7] compares the theoretical prediction with experimental data for brass, magnesium, stainless-steel, and rough aluminum surfaces, showing the good agreement obtained. Note that it is not an easy task to measure the parameter $\frac{b_L}{d_t}$ that is obtained from the study of the profile of the contacting surfaces from a profilometer reading.

Empirical Correlations

Two main types of correlations are found in the literature: those between the semiempirical correlations based on theory (presented previously) and experimental data, and the fully empirical correlations based only on experimental data. Usually, the expressions resulting from the correlations are simple and easy to use,

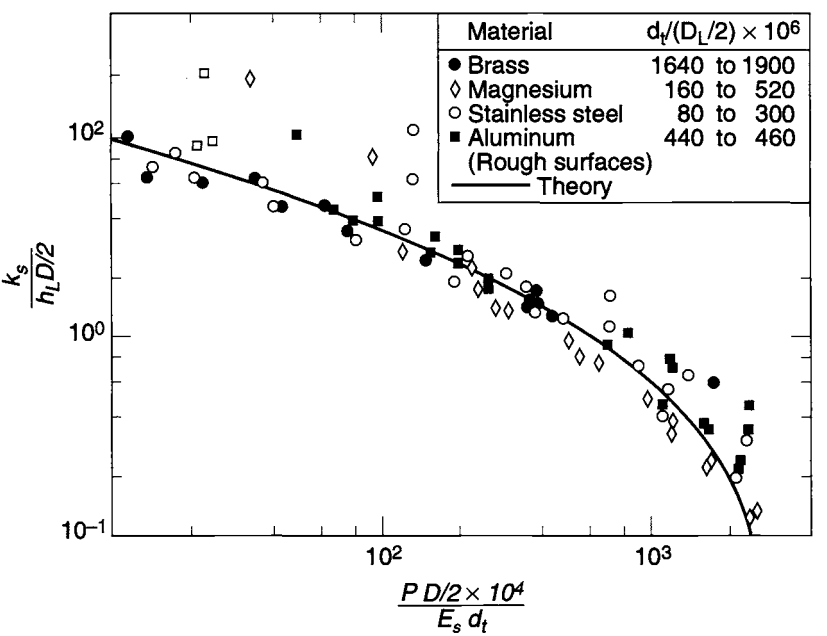

Fig. 16.11. Comparison between the Clausing and Chao[16.7] wavy rough contact correlation and data. (Courtesy of NASA)

as they require few input parameters. However, they are valid for a limited range of contacts. Fully empirical correlations can be applied only to contacts similar to those from which they were generated. Semiempirical ones can be applied to a larger range of contacts, especially when the user is aware of the theory behind the correlation.

Lambert and Fletcher[16.24] presented a review of the correlations available in the literature for thermal contact resistance. They made an interesting comparison of these correlations with the experimental data of Hegazy.[16.3] They concluded that the correlations that include gap conductance (which is negligible in vacuum conditions) do not compare well with vacuum data.

The authors also have shown that most of the Russian correlations are approximate to Hegazy's data only for very rough surfaces. Rough surfaces are relatively unworked, since they are not strain-hardened from machining processes. The Russian researchers assumed that the contact hardness is approximately equal to the bulk hardness. As explained earlier in this chapter, Mikic, Yovanovich, Hegazy, and many other investigators believe that the microhardness is a much more appropriate contact-deformation parameter. Lambert and Fletcher (1996) verified that, among the Russian correlations, Popov's correlations perform well for both smooth Ni 200 and rough SS 304. The Popov correlation expression was obtained for 80 data points for a variety of materials, for nominally flat rough surfaces where σ is assumed to be 30 μm. The relation is:

$$h_c = 2.7\times10^4 k_s \left(\frac{C_1 P}{3S_U}\right)^{0.956} \tag{16.62}$$

$$C_1 = 12/(\sigma_{1,\max} + \sigma_{2,\max}) \; for \; 1\mu m \le \sigma_{1,\max} + \sigma_{2,\max} < 5\mu m \tag{16.63}$$

$$C_1 = [20/(\sigma_{1,\max} + \sigma_{2,\max})]^{0.63} for \; 5\mu m \le \sigma_{1,\max} + \sigma_{2,\max} < 10\mu m \tag{16.64}$$

$$C_1 = [30/(\sigma_{1,\max} + \sigma_{2,\max})]^{0.4} for \; 10\mu m \le \sigma_{1,\max} + \sigma_{2,\max} < 30\mu m \tag{16.65}$$

where S_U is the ultimate strength of the softer metal.

Lambert and Fletcher[16.24] also observed that the O'Callaghan and Probert (1974) empirical correlation agrees well with Hegazy's data for rough surfaces at low contact pressure. The O'Callaghan and Probert[16.25] expression, obtained for 344 aluminum data, for flat, rough surfaces, is:

$$h_c = 3.73 k_s \frac{\sigma}{A}\left(\frac{P\cdot A}{\sigma^2 H}\right)^{0.66} \tag{16.66}$$

Typical Experimental Setup

Experimental measurements of thermal contact resistance for use in spacecraft thermal analysis must be obtained in vacuum. Basically, all the data presented in this section were measured with an experimental setup very similar to the one described here and depicted in Fig. 16.12. A detailed description of a sample setup can be found in Nho.[16.21] In this case, the test column is enclosed within a Pyrex bell jar and a base plate. The test column consists of the heater block, the heat

meter, the upper and lower test specimens, the heat sink, and the load cell. The gas pressure within the bell jar is controlled by a vacuum system, which is a mechanical pump connected in series with an oil-diffusion pump. A vacuum level lower than 10^{-5} torr should be achieved. The heater may consist of two cartridge-type heaters embedded into a brass block. A closed-loop thermobath should be used to cool the aluminum cold plate. The load is applied to the test column with the aid of a diaphragm-type air cylinder. A calibrated load cell is used to measure the applied load. The mechanical loads, heater levels, and data acquisition can be controlled with a personal computer.

The Effect of Oxidation on Thermal Contact Resistance

Bare surfaces may oxidize when in contact with air, creating a very thin layer of low-conductivity material. The presence of oxides usually increases the thermal contact resistance because the oxides are harder and have lower conductivities than the substrate material.

Yip[16.26] studied, theoretically and experimentally, the effect of oxide films on thermal contact resistance. His model showed good agreement with his data and with another model, developed by Al-Astrabadi *et al.*[16.27] Only the latter model is presented here because it requires less computational effort. Figure 16.13 shows a schematic of the contact between nominally flat, randomly rough, and oxidized metallic surfaces.

The model of Al-Astrabadi *et al.*[16.27] uses a stochastic representation of the surface microtopography and assumes a uniform oxide film of thickness t. The

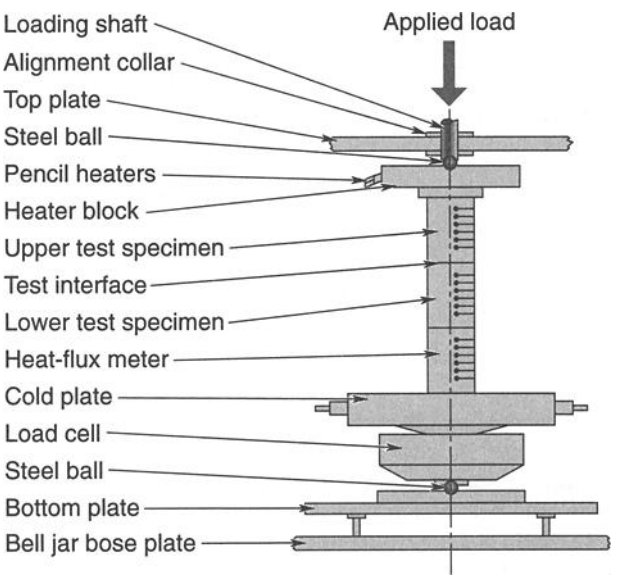

Fig. 16.12. Thermal contact conductance measurement experimental setup.

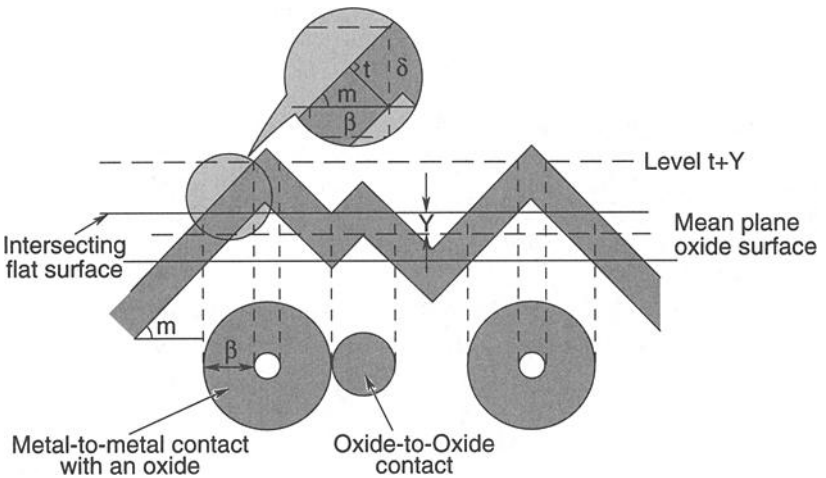

Fig. 16.13. Idealized contact of oxidized surfaces.

microcontacts are of two types—metal-to-metal bridges, surrounded by contacting annular oxide areas, and oxide-to-oxide bridges. All the microcontact regions are taken to be circular, and the asperities are assumed to be circular cones that deform plastically. The effective thermal conductivity of the oxide-to-oxide microcontact is given by the harmonic mean of the conductivities of the oxide and metal, $k_{co}= \dfrac{2k_m k_o}{k_m+k_o}$, while the effective thermal conductivity of the metal-to-metal contact surrounded by an annulus of oxide is given by the arithmetic mean of the conductivities of the oxide and metal, $k_{cm}= \dfrac{k_m + k_o}{2}$. In these equations, the subscript m refers to metal and o to oxide. The total resistance consists of two thermal resistances in parallel: the oxide-to-oxide resistance R_{co} and the metal-to-metal resistance R_{cm}, given respectively by

$$R_{co}= \frac{\psi}{2a_o n_o k_{co} A_a} \text{ and } R_{cm}= \frac{\psi}{2a_m n_m k_{cm} A_a} \tag{16.67}$$

Then, the total contact resistance is

$$R_c= \left(\frac{1}{R_{co}} + \frac{1}{R_{cm}}\right)^{-1} \tag{16.68}$$

The value of the parameter ψ is given by Eq. (16.15), where a/b represents the ratio of the mean radii between the microcontact spot and the heat-flow channel to the parameter b, which is determined by Eq. (16.23). The total number of contacts per unit apparent area n_t, including oxide-to-oxide n_o and metal-to-metal n_m, is:

$$n_t a_t= n_m a_m + n_o a_o \tag{16.69}$$

On the other hand, the stochastic asperities-distribution model results in the following expression for the determination of the total number of contacts:

$$n_t = \left(\frac{1}{8}\sqrt{\frac{\pi}{2}}\frac{Y}{\sigma} m^2 e^{-\frac{1}{2}\left(\frac{Y}{\sigma}\right)^2} \right) \tag{16.70}$$

For the number of metal-to-metal contacts:

$$n_m = \frac{1}{8}\sqrt{\frac{\pi}{2}}\left(\frac{Y}{\sigma} + \delta\right) m^2 e^{-\frac{1}{2}\left(\frac{Y}{\sigma} + \delta\right)^2} \tag{16.71}$$

In Fig. 16.13, t is the oxide thickness in the slope direction of the surface, δ is its vertical projection, and β is the lateral spread of oxide surrounding each metal-to-metal contact spot. Values for δ and β are given by:

$$\delta = \frac{t}{\sigma\cos(|m|)} \quad \text{and} \quad \beta = \frac{t}{\sigma\sin(|m|)} \tag{16.72}$$

The number of oxide-to-oxide contacts per unit apparent area is:

$$n_o = n_t - n_m \tag{16.73}$$

The overall mean radius of the microcontact spot, a_t, is:

$$a_t = \frac{2\sigma}{\pi m \frac{Y}{\sigma}} \tag{16.74}$$

The metal-to-metal mean radius, a_m, is:

$$a_m = \frac{2\sigma}{\pi m\left(\frac{Y}{\sigma} + \delta\right)} + \beta\sigma \tag{16.75}$$

Finally, the normalized Y/σ and/or the mean plane separation Y are determined by the solution of this transcendental equation:

$$\left[\frac{1}{2} - \frac{1}{\sqrt{2\pi}} e^{-\frac{1}{2}\left(\frac{Y}{\sigma} + \delta\right)}\right] + \left[\frac{1}{\sqrt{2\pi}} e^{-\frac{1}{2}\left(\frac{Y}{\sigma} + \delta\right)^2} - \frac{1}{2} e^{-\frac{1}{2}\left(\frac{Y}{\sigma}\right)^2}\right]\frac{H_o}{H_m} = \frac{P}{H_m} \tag{16.76}$$

Al-Astrabadi *et al.*[16.27] conducted experiments to verify their theory using mild steel (EN3B) specimens with surface roughness ranging from approximately 0.12 to 2 μm, asperity slopes between 0.04 and 0.19 rad, and an oxide film thickness of 0.055 to 0.118 μm. The comparison between data and model was quite good. They noted that oxidation of the surfaces had a minimal effect on the surfaces' topography. They stated that the following three ratios influence the contact resistance: the ratio of coating to substrate hardness, the ratio of coating to substrate thermal conductivity, and the ratio of coating thickness to surface roughness. They

postulated that, if the coating is much thicker than the roughness, then the resistance increases with increasing coating thickness. Provided that the coating thickness is on the order of, or less than, the roughness, the resistance will decrease if the coating is much softer than the substrate.

Lambert *et al.* performed an experimental investigation of the thermal contact conductance of different anodized coatings. They concluded that the overall conductance of anodic coatings is greatly affected by coating thickness. They tested coatings with thickness greater than the average surface roughness of the underlying substrates, prior to anodization.

The Effect of Interstitial Materials on Thermal Contact Resistance

For space applications, low-resistance junctions are designed to provide a good thermal coupling between a heat source, such as an electronics box, and a heat sink, such as a shelf or radiator. Several techniques can be applied to decrease the thermal resistance of the contacting surfaces of these joints, including insertion of a soft foil between the contacting surfaces or application of a coating on one or both of the contacting surfaces. Several coating materials can be applied: vaporized metals, ceramics, diamondlike films, plastics, etc.

Modeling the contact resistance of such a junction is a difficult task, because the model must take into account the material of the coating and the substrate and their thermophysical and geometric properties. Some theoretical models can be found in the literature for the determination of the thermal contact resistance of these joints. They are not general; i.e., they are valid only for specific coatings and substrates. This section presents only the models that are easy to employ.

Foils

Any interstitial substance that is softer than the contacting surfaces will significantly increase the contact-spot density and also increase the contact-spot radius, thereby decreasing the joint resistance. The interstitial spaces are partially filled, and the result is an increased contact area. Yovanovich[16.28] has shown that the thermal performance of a foil depends primarily on the ratio of the foil's thermal conductivity to its microhardness. The higher this index, the better the foil's performance. The thickness of the foil is also critical to the performance, and for a given material an optimum foil thickness exists. Yovanovich tested Armco iron contacting-surface samples where lead, tin, aluminum, and copper were inserted in the joint. Figure 16.14, which is typical for all foil materials tested, shows the joint resistance of the tinfoil mounting as a function of the foil thickness for the joint subjected to five different levels of contact pressure. The joint resistance consists of two contact resistances and the foil material resistance in series. Chapter 8 discusses interstitial materials commonly used in spacecraft thermal control and provides general conductance values for such thermal joints.

Metallic Coating Model

Antonetti[16.22] and Antonetti and Yovanovich[16.29] provided a complete treatment of the thermal and mechanical problem associated with thermal contact resistance

of coated surfaces. The model presented in this subsection is valid for conforming rough surfaces.

Figure 16.15 shows a schematic of a contact between a flat smooth surface coated with a soft metallic layer of high conductivity and a flat rough surface. The prime parameters in the following equations are associated with the contact conductances for coated surfaces. The general expression for the contact conductance of this joint operating in vacuum is

$$h_c' = h_c\left(\frac{H}{H'}\right)^{0.93}\left[\frac{k_1 + k_2}{Ck_1 + k_2}\right] \tag{16.77}$$

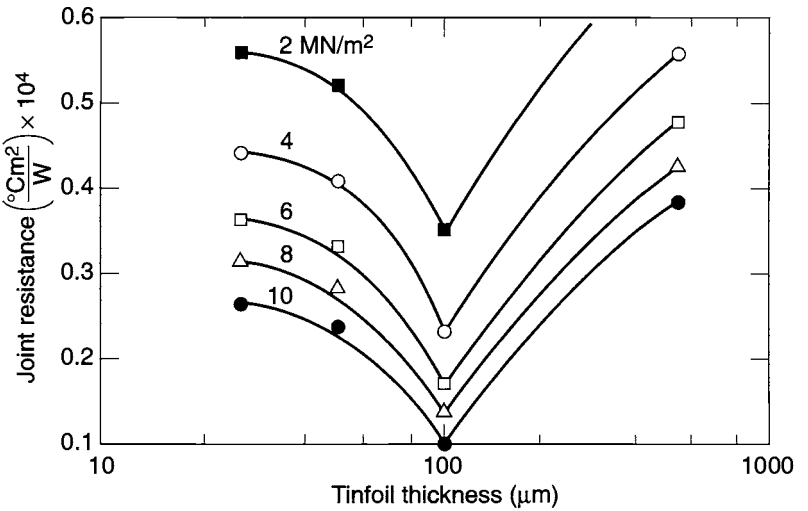

Fig. 16.14. Effect of the metallic foil thickness on joint resistance.

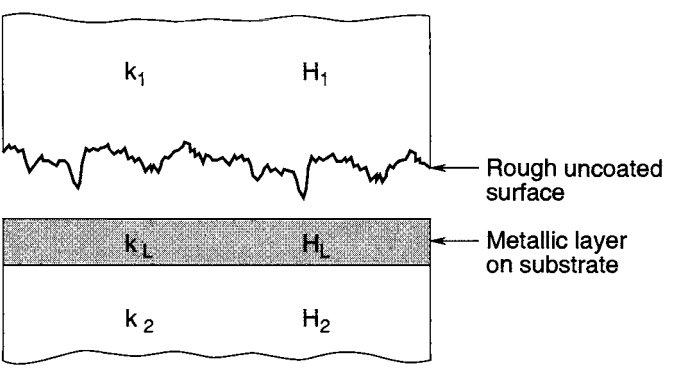

Fig. 16.15. Schematic of the coated joint.

where H' is the effective microhardness of the layer-substrate combination and C is a constriction-parameter correction factor that accounts for the heat spreading in the coated surface.

As can be seen from Eq. (16.77), the coated contact conductance is the product of three quantities: the uncoated contact conductance, h_c, a mechanical modification factor, $\left(\frac{H}{H'}\right)^{0.93}$, and the thermal modification factor, which is displayed in brackets. The uncoated conductance can be determined by evaluating Eq. (16.34). Therefore, for a given joint, the only unknowns are the effective microhardness, H', and the constriction-parameter correction factor, C. They are the key to solving contact problems with coated surfaces.

Mechanical Model

The best way to obtain the effective microhardness is to perform the Vickers measurement of the combination layer (coating)-substrate. This measurement will result in a plot of the effective microhardness as a function of the relative layer thickness (ratio between thickness of the layer and equivalent Vickers indentation depth, *t/d*), similar to that of the silver layer on a nickel substrate, as shown in Fig. 16.16.

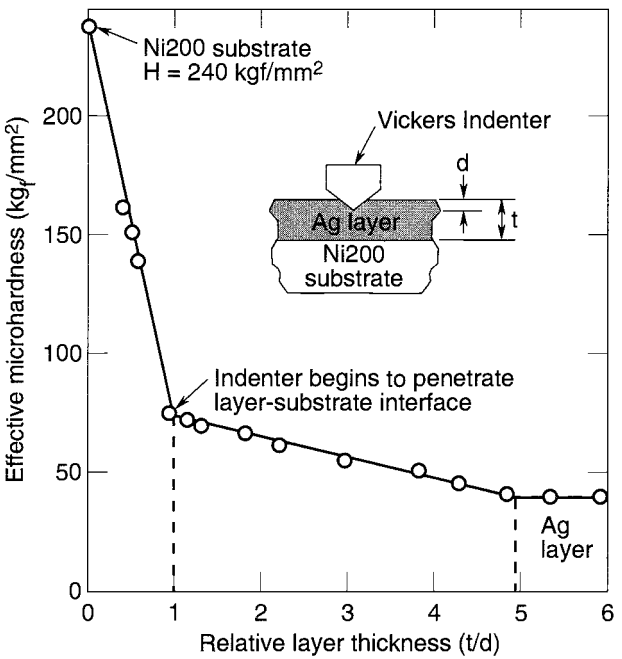

Fig. 16.16. Vickers microhardness measures for silver layer on Nickel 200 substrate.

When Vickers microhardness measurements are not available, for a first approximation, one assumes that the general form of the plot for the particular layer-substrate combination under consideration is similar to that shown in Fig. 16.16, and the following equations can be used to estimate the effective microhardness. For $t/d < 1.0$ (Antonetti[16.22]):

$$H' = H_2\left(1 - \frac{t}{d}\right) + 1.81H_L\left(\frac{t}{d}\right) \tag{16.78}$$

where H_L is the microhardness of the layer and H_2 is the bulk microhardness of the substrate, both obtained from the Vickers microhardness test. For $1.0 \leq t/d \leq 4.90$:

$$H' = 1.81H_L - 0.21H_L\left(\frac{t}{d} - 1\right) \tag{16.79}$$

where the relative thickness t/d is determined from:

$$\frac{t}{d} = 1.04\frac{t}{\sigma}\left(\frac{P}{H'}\right)^{-0.097} \tag{16.80}$$

When $t/d > 4.90$, the effective microhardness is equal to the layer microhardness H_L.

As t/d depends upon the effective microhardness and t/d must be known to determine the effective microhardness, an iterative approach is required. If the arithmetic average of the layer and substrate microhardness values is used as the initial guess, the convergence is rapid. If the substrate surface has been work-hardened, then use of the substrate bulk hardness is incorrect. Yovanovich, Hegazy, and De Vaal[16.30] proposed a method to determine a proper value of the effective microhardness.

Thermal Model

Antonetti[16.22] solved Laplace's equation for the temperature distributions within the layer and substrate subjected to the perfect contact boundary condition at their common interface. For the constriction resistance as defined in Eq. (16.8), the constriction parameter for a coated surface is shown to be:

$$\psi' = \frac{16}{\pi\varepsilon'}\sum_{n=1}^{\infty}\left[\frac{J_1^2(\lambda_n b'\varepsilon')}{(\lambda_n b')^3 J_0^2(\lambda_n b')}\right]\phi_n\gamma_n\rho_n \tag{16.81}$$

The first term to the right of the sigma in Eq. (16.81), the term in brackets, represents a dimensionless constriction parameter for an uncoated contact (considering uniform heat-flux conditions at the contact area); the second, ϕ_n, accounts for the influence of the layer; the third term, γ_n, accounts for the contact temperature basis used to determine the constriction resistance; and the fourth, ρ_n, accounts for the contact-spot heat-flux distribution. The eigenvalues λ_n are the roots of the equation $J_1(b'\lambda_n) = 0$. For adjoining surfaces, the contact spots are assumed to be isothermal. The modification factors in this case are $\gamma_n = 1$,

$$\phi_n = K\left[\frac{(1+K)+(1-K)e^{-2\lambda_n a'\tau}}{(1+K)-(1-K)e^{-2\lambda_n a'\tau}}\right], \tag{16.82}$$

and

$$\rho_n = \frac{\sin(\lambda_n b'\varepsilon)}{2J_1(\lambda_n b'\varepsilon)}, \tag{16.83}$$

where $\tau = \frac{t}{a'}$ is the relative layer thickness and K is the ratio of the substrate to layer conductivities. The constriction-parameter correction factor, C, is defined as the ratio of the constriction parameter with a layer [Eq. (16.81)] to that without a layer [Eq. (16.9) or (16.15)], for the same value of the relative contact-spot radius.For isothermal contact temperature, typical values are presented in Table 16.2. A more complete table for this factor can be found in Antonetti.[16.22]

Antonetti[16.22] also developed an alternative contact-conductance model, based on the Yovanovich[16.18] correlation [Eq. (16.34)]. Based on the expression on the left side of Eq. (16.81), considering that there are two constriction resistances in series (surfaces 1 and 2), for N contact spots in parallel, one finds the contact conductance for a coated contact:

$$h'_c = \frac{2a'k'}{\psi(\varepsilon')}\left(\frac{N}{A_a}\right) \tag{16.84}$$

where k' is based on Eq. (16.77) and is defined as

$$k' = \frac{2k_1k_2}{C_2k_1 + k_2}. \tag{16.85}$$

Equation (16.9) can also be used to determine the constriction parameter. The average contact-spot radius parameter can be determined from

$$a' = 0.77\left(\frac{\sigma}{m}\right)\left(\frac{P}{H'}\right)^{0.097}. \tag{16.86}$$

Table 16.2. Thermal Constriction Resistance Parameter Correction Factor

e	1/K	t/a	C
0.005	2	0.01	0.9842
0.200	2	0.50	0.6218
0.500	50	0.05	0.0260

By means of a force balance at the joint, the total number of contact spots per unit apparent area can be estimated by

$$\frac{N'}{A_a} = \frac{1}{\pi(a')^2}\left(\frac{P}{H'}\right). \tag{16.87}$$

Although Eqs. (16.77) and (16.84) differ algebraically, they yield the same numerical results. The advantage of Eq. (16.77) is that it permits the researcher to appreciate how the various parameters contribute to the coated contact conductance.

Antonetti[16.22] demonstrated that the bare conforming rough surface model of Cooper *et al.*[16.4] that was correlated by Yovanovich[16.18] can be used to correlate the contact with coated surfaces:

$$\frac{h'_c\sigma}{k'm} = 1.25\left(\frac{P}{H'}\right)^{0.95} \tag{16.88}$$

Antonetti[16.22] and Antonetti and Yovanovich[16.29] experimentally verified their model, performing thermal tests with Nickel 200 specimens. One of the specimens was coated with a thin layer of pure silver and the other was bead-blasted to different levels of roughness. The authors verified that the joint conductance was increased approximately by a factor of 10 when the layer is around 6 μm thick, for a surface having a roughness of 1.28 μm. The good agreement between the theory and data can be observed in the plot of the dimensionless thermal conductance, defined as $\frac{h_c'\sigma}{mk'}$ against the relative pressure $\frac{P}{H'}$ [H' is given by Eqs. (16.78) and (16.79)], presented in Fig. 16.17.

Experimental Data

Several publications deal with experimental measurements of the thermal resistance of contacting surfaces, where at least one of the surfaces is coated. In most cases, the coating is applied with the objective of enhancing the overall thermal conductance of the joint. Some of these experiments, which can be useful for satellite applications, are presented here.

Metallic Coatings

Kang *et al.*[16.31] studied the contact conductance of Aluminum 6061-T6 surfaces, where metallic coatings were vapor-deposited. Lead, tin, and indium were evaluated using four different coating thicknesses: 2.0 to 3.0 μm for indium, 1.5 to 2.5 μm for lead, and 0.2 to 0.5 μm for tin. The enhancement factors for the thermal contact conductance were found to be on the order of 700, 400, and 50%, respectively.

Chung *et al.*[16.32] (1993) studied the thermal contact conductance of a phase-mixed coating layer applied over metallic surfaces using a transitional technique that consists of a plasma-enhanced deposition onto a cold surface. Their experimental study was restricted to a relatively low ratio of the contact pressure to the

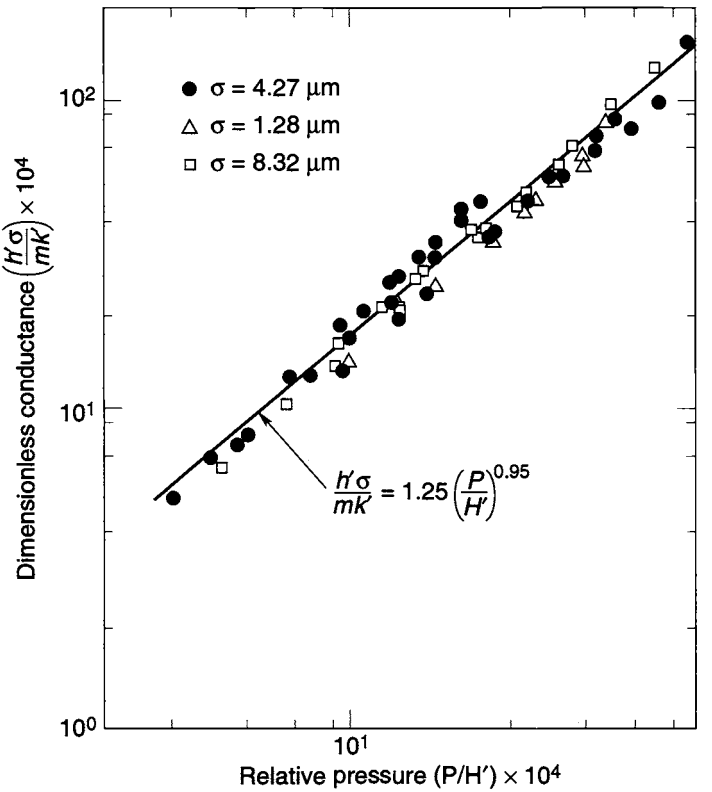

Fig. 16.17. Dimensionless contact conductance versus relative contact pressure for silver layer on nickel substrate.

microhardness $\left(10^{-4} < \frac{P}{H} < 6\times10^{-4}\right)$, where very few data exist. They coated Aluminum 6061-T6 surfaces with pure copper, pure silver, a phase mixture of copper and carbon, and another of silver and carbon. Actually, the pure layers yielded 10 to 30% higher values of the contact conductance when compared with the carbon mixtures. The researchers justified the use of phase-mixed coatings by the improvement of the mechanical properties of the coating.

Howard and Peterson[16.33] studied the effect of multiple layering on the thermal contact conductance of vapor-deposited metallic coatings. They concluded that oxidation and thermal cycling intrinsic to the mechanical coating process cause poor layer adhesion that resulted in a significantly smaller enhancement factor than that occurring from single-layer coatings with an equivalent thickness.

Lambert and Fletcher[16.34] observed that the literature models are valid for optically flat idealized surfaces, which are hard to find in engineering. They collected and correlated a large body of conductance data of contacts involving wavy and

rough engineering surfaces, obtained from different laboratories, resulting in the expression:

$$\frac{h'_c\sigma}{k'm} = 0.00503\left(\frac{P}{H'}\right)^{0.455} \tag{16.89}$$

This correlation presents a significantly smaller $\left(\frac{P}{H'}\right)$ exponent (0.455) than that predicted by Antonetti and Yovanovich[16.35] [0.95, Eq. (16.88)], indicating that nonflat wavy surfaces are less sensitive to contact pressure than the optically flat surfaces.

Li *et al.*[16.36] experimentally investigated four coating materials: tin, copper, aluminum, and silver. Two methods of coating were used, electroplating and filtered arc vapor deposition, and the experiments verified that optimum coating thickness varies according to the selected material. This thickness is determined by the hardness: the harder the coating material, the thicker the coating needs to be for better performance. Therefore, the authors suggested, the parameter k/H could be used to rank the coating material. They also concluded that the maximum enhancement of contact conductance is obtained when both contacting surfaces are coated. They observed that the enhancement factor, which ranges from 4 to 21, is a function of the contact pressure.

Other experimental conductance measurements of contacts where the surfaces are metal-coated can be found in the extensive literature review made by Lambert and Fletcher.[16.37] They also compared and ranked the thermal performance of the coating materials.

Nonmetallic Coatings

Marotta *et al.*[16.38] made a literature review of experimental data available for the thermal contact conductance of nonmetallic coatings, which they classified in four groups: oxides, carbon-based coatings, ceramics, and polymer-based coatings. The oxide films were already treated. Carbon-based coatings, such as polycrystalline diamondlike films, offer excellent thermophysical properties, which make them attractive coatings. The deposition temperatures of polycrystalline diamondlike films (770–900 K) limit the deposition of these films to metals that can withstand high temperatures without loss of mechanical properties. Ceramics generally exhibit good structural and thermal capabilities at high temperatures. They resist oxidation, erosion, and corrosion, and they wear more than most metals. Some of the ceramics tested are: titanium nitrite (TiN), titanium carbide (TiC), and silicon carbide (SiC). They can be applied to complex shapes. Impregnation coatings (synergistic) combine the properties of two or more materials to provide a surface with permanent dry lubricity, added wear, corrosion resistance, and high chemical inertness. Marotta and Fletcher[16.39] presented many experimental data obtained from their own experimental work on thermal contact conductance of a ceramic coating deposited on aluminum 6061-T6 and copper CC11000-H03. Marotta *et al.*[16.40] (1996) also conducted experiments on thermal contact conductance of diamondlike films deposited over these same materials (aluminum and

copper). Their studies confirmed and completed the information gathered from the literature.

The experimental work presented in this section for contact with nonmetallic coatings was intended for terrestrial applications. This technology is promising for space but should be tested accordingly before being applied.

Nomenclature

a	contact-spot radius
A	contact area
b	elemental heat-flux tube radius
c	geometry parameter as defined in Fig. 16.4(b)
C	ratio of the constriction parameter with a layer to that without a layer
C_1	Vickers correlation coefficient, correlation parameter
C_2	Vickers correlation coefficient
d	geometry parameter as defined in Fig. 16.4(b), height of the waviness represented by a spherical crown, Vickers indentation depth
D	diameter of the contour area
E	modulus of elasticity
f_{ep}	elastoplastic factor
g	contour area function
h	conductance
H	surface microhardness
J_o,J_1	Bessel functions
k	conductivity
K	ratio of the substrate to layer conductivities
L	wavelength of the spherical waviness
m	surface slope
n	number of microcontacts per unit apparent area
N	number of contact spots
p	probability density function
P	contact pressure
Q	heat flux
r	radius
R	thermal resistance
S_f	flow stress
S_U	ultimate strength
t	thickness
T	temperature
x	relative mean plane separation
$y(x)$	surface profile height
Y	mean plane separation height

Nomenclature—*Continued*

z	axial direction

Greek Letters

β	lateral spread of oxide
δ	oxide layer thickness vertical projection
ε	relative real contact area
Φ_n	uncoated contact dimensionless constriction parameter
γ_n	layer influence parameter
η	elastoplastic index
λ	contour area, eigenvalue
ρ_n	contact-spot heat-flux distribution
σ	standard mean height deviation (root mean square deviation)
τ	relative layer thickness
υ	Poisson's ratio
ξ	elastic deformation factor
Ψ	constriction parameter

Subscripts and Superscripts

a	apparent
c	contact
cm	metal-to-metal
co	oxide-to-oxide
e	elastic
eff	effective
ep	elastoplastic
g	gas
H	bulk
j	joint
L	large, layer
m	metal
max	maximum
o	oxide
r	radiation, real
s	microconstriction, harmonic mean
t	total
0	initial
1,2	surface
	coating

References

16.1. T. H. McWaid, "Thermal Contact Resistance Across Pressed Metal Contact in a Vacuum Environment," Ph. D. thesis, University of Waterloo, Canada, 1990, pp. 1–264.

16.2. S. Song and M. M. Yovanovich, "Relative Contact Pressure: Dependence on Surface Roughness and Vickers Hardness," *AIAA Journal of Thermophysics* **2** (1), 43–47 (January 1988).

16.3. A. A. Hegazy, "Thermal Joint Conductance of Conforming Rough Surfaces," Ph.D. thesis, University of Waterloo, Canada, 1985.

16.4. M. G. Cooper, B. B. Mikic, and M. M. Yovanovich, "Thermal Contact Conductance," *International Journal of Heat and Mass Transfer* **12**, 279–300 (1969).

16.5. B. B. Mikic and W. M. Rohsenow, "Thermal Contact Resistance," Technical Report No. 4541-41, Massachusetts Institute of Technology, Cambridge, MA, 1966, pp. 1–129.

16.6. L. C. Roess, "Theory of Spreading Conductance," appendix to N. D. Weills and E. A. Ryder, "Thermal Resistance Measurements on Joints Formed between Stationary Metal Surfaces," *Semi-Annual ASME Heat Transfer Divison Meeting* (Milwaukee, WI, 1948).

16.7. A. M. Clausing and B. T. Chao, "Thermal Contact Resistance in a Vacuum Environment," *Journal of Heat Transfer*, 243–251 (May 1965).

16.8. A. M. Clausing, "An Experimental and Theoretical Investigation of the Thermal Contact Resistance," Semi-Annual Status Report Number 8: Research Grant NASA NsG 242, University of Illinois, 1965, pp. 1–23.

16.9. M. M. Yovanovich, "Overall Thermal Resistance between Contacting Rough, Wavy Surfaces," *International Journal of Heat and Mass Transfer* **12**, 1517–1520 (1969).

16.10. S. S. Burde and M. M. Yovanovich, "Thermal Resistance at Smooth-Sphere / Rough-Flat Contacts: Theoretical Analysis," *Progress in Astronautics and Aeronautics: Thermophysics and Thermal Control* **65**, 83–102 (1978).

16.11. M. A. Lambert and L. S. Fletcher, "Thermal Contact Conductance of Spherical Rough Metals," *Journal of Heat Transfer* **119**, 684–690 (November 1997).

16.12. B. B. Mikic, "Thermal Constriction Resistance Due to Non-Uniform Surface Conditions: Contact Resistance at Non-Uniform Interface Pressure," *International Journal of Heat and Mass Transfer* **13**, 1497–1500 (1970).

16.13. M. Sridhar and M. Yovanovich, "Critical Review of Elastic and Plastic Thermal Contact Conductance Models and Comparison with Experiment" *AIAA 28th Thermophysics Conference* (Orlando, FL, July 1993), pp. 1–14.

16.14. B. B. Mikic, "Thermal Contact Conductance; Theoretical Considerations," *International Journal of Heat and Mass Transfer* **17**, 205–212 (1974).

16.15. M. R. Sridhar, "Elastoplastic Contact Models for Sphere—Flat and Conforming Rough Surface Applications," Ph. D. thesis, University of Waterloo, Canada, 1994, pp. 1–332.

16.16. B. B. Mikic, M. M. Yovanovich, and W. M. Rohsenow, "The Effect of Surface Roughness and Waviness Upon the Overall Thermal Contact Resistance," Technical Report No. 76361-43, Massachusetts Institute of Technology, Cambridge, MA, 1966, pp. 1–94.

16.17. J. A. Greenwood and J. B. P. Williamson, "Contact of Nominally Flat Surfaces," *Proceedings of the Royal Society, Vol. A-295* (The British Library—Photocopy Service, 1966), pp. 300–319.

16.18. M. M. Yovanovich, "Thermal Contact Correlations," *Spacecraft Radiative Transfer and Temperature Control, Astronautics and Aeronautics* **83**, 83–95 (1982).

16.19. B. B. Mikic, "Analytical Studies of Contact Nominally Flat Surfaces; Effect of Previous Loading" *Journal of Lubrication Technology*, 451–456 (October 1971).

16.20. M. R. Sridhar and M. M. Yovanovich, "Elastoplastic Contact Conductance Model for Isotropic Conforming Rough Surfaces and Comparison with Experiments," *Thermal Phenomena at Molecular and Microscales and in Cryogenic Infrared Detectors, ASME HTD* **277**, 43–56 (1994).

16.21. K. M. Nho, "Experimental Investigation of Heat Flow Rate and Directional Effect on Contact Conductance of Anisotropic Ground/Lapped Interfaces," Ph. D. thesis, University of Waterloo, Canada, 1990, pp. 1–291.

16.22. V. W. Antonetti, "On the Use of Metallic Coatings to Enhance Thermal Contact Conductance," Ph. D. thesis, University of Waterloo, Canada, 1983, pp. 1–198.

16.23. R. Holm, *Electrical Contacts Handbook*, 3rd ed. (Springer Handbook, Berlin, 1958).

16.24. M. A. Lambert and L. S. Fletcher, "A Review of Models for Thermal Contact Conductance of Metals," *34th Aerospace Sciences Meeting & Exhibit* (Reno, NV, 15–18 January, 1996).

16.25. P. W. O'Callaghan and S. D. Probert, "Effects of Static Loading on Surfaces Parameters," *Wear*, Elsevier Sequoia S. A., Netherland **24,** 133–145 (1973).

16.26. F. C. Yip, "The Effect of Oxide Films on Thermal Contact Resistance," *AIAA/ ASME Thermophysics Specialist Conference* (Boston, MA, July 1974), pp. 1–8.

16.27. F. R. Al-Astrabadi, P. W. O'Callaghan, and S. D. Probert, "Thermal Resistance of Contacts: Influence of Oxide Films," *AIAA 15th Thermophysics Conference* (Snowmass, Aspen, CO, July 1980), pp. 267–283.

16.28. M. M. Yovanovich, "Effect of Foils upon Joint Resistance: Evidence of Optimum Thickness," *AIAA Progress in Astronautics and Aeronautics: Thermal Control and Radiation, Vol. 31*, edited by Chang-Lin Tien (New York, 1973).

16.29. V. W. Antonetti and M. M. Yovanovich, "Enhancement of Thermal Contact Conductance by Metallic Coatings: Theory and Experiments," *Journal of Heat Transfer* **107**, 513–519 (1985).

16.30. Yovanovich, Hegazy, and De Vaal (1982).

16.31. T. K. Kang, G. P. Peterson, and L. S. Fletcher, "Effect of Metallic Coatings on the Thermal Contact Conductance of Turned Surfaces," *Journal of Heat Transfer* **112**, 864–871 (November 1990).

16.32. K. C. Chung, J. W. Sheffield, H. J. Sauer Jr., and T. J. O'Keefe, "Thermal Contact Conductance of a Phase-Mixed Coating Layer by Transitional Buffering Interface," *Journal of Thermophysics and Heat Transfer* **7** (2), 326–333 (April–June 1993).

16.33. A. H. Howard and G. P. Peterson, "The Effect of Multiple Layering on the Thermal Contact Conductance of Vapor Deposited Metallic Coatings," *AIAA 31st Aerospace Sciences Meeting & Exhibit*, (Reno, NV, January 1993), pp. 1–7.

16.34. M. A. Lambert and L. S. Fletcher, "A Correlation for the Thermal Contact Conductance of Metallic Coated Metals," *AIAA 28th Thermophysics Conference*, (Orlando, FL, July 1993), pp. 1–8.

16.35. V. W. Antonetti and M. M. Yovanovich, "Thermal Contact Resistance in Microelectronic Equipments," *International Journal Hybrid Microelectronics* **7**, 44–50 (1984).

16.36. Y. Z. Li, C. V. Madhusudana, and E. Leonardi, "Enhancement of Thermal Contact Conductance: Effect of Metallic Coating," *Journal of Thermophysics and Heat Transfer* **14** (4), 540–547 (October–December 2000).

16.37. M. A. Lambert and L. S. Fletcher, "Review of the Thermal Contact Conductance of Junctions with Metallic Coatings and Films," *Journal of Thermophysics and Heat Transfer* **7** (4), 547–554 (October–December 1993).

16.38. E. E. Marotta, M. A. Lambert, and L. S. Fletcher, "A Review of the Thermal Contact Conductance of Non-Metallic Coating and Films," *AIAA 27th Thermophysics Conference*, (Nashville, TN, July 1992), pp. 1–17.

16.39. E. E. Marotta and L. S. Fletcher, "Thermal Contact Conductance of Refractory Ceramic Coatings," *Journal of Thermophysics and Heat Transfer* **10** (1), 10–18 (January–March 1996).

16.40. E. E. Marotta, L. S. Fletcher, and D. G. Blanchard, "Thermal Contact Conductance of Diamond-Like Films," *Journal of Thermophysics and Heat Transfer* **10** (1), 19–25 (January–March 1996).